Turbulent flow analysis and cavitation prediction in axial cooling water pump

Yousef Vazifeshenas[1], Mousa Farhadi[2,*], Kurosh Sedighi[3] and Ruzbeh Shafaghat[4]

[1]MSc student, Faculty of Mechanical Engineering, Babol University of Technology; (joseph.vazifeshenas@gmail.com)

[2]Associate Professor, Faculty of Mechanical Engineering, Babol University of Technology. P. O. Box 484

[3] Associate Professor, Faculty of Mechanical Engineering, Babol University of Technology;
(ksedighi@nit.ac.ir)

[4]Assistant Professor, Faculty of Mechanical Engineering, Babol University of Technology
(rshafaghat@nit.ac.ir)

ABSTRACT

The aim of this literature is to investigate the performance and three-dimensional flow field in an axial flow CW pump and observing cavitation phenomenon in specified situations. Computational Fluid Dynamic software FLUENT 6.3 was utilized to simulate the whole flow field of the pump to capture all features in the domain. RNG k-ε model combined with standard wall functions is used to deal with the turbulent nature of the problem. Two principal domains are verified: 1) the rotor domain which includes four moving impellers. 2) the stator domain which includes nine static vanes. Hence, the rotor-stator interaction was treated with Moving Reference Frame (MRF) technique. Pressure contour and streamlines of the simulation are shown here. The performance curve of the model is in good agreement with the reference power plant data. Finally, the cavitation region defined with the vaporization pressure is demonstrated for cases with different flow rates.

Keywords: Axial flow pump, Turbulence, Moving reference frame, CFD, Cavitation

1. INTRODUCTION

Large scale industrial pumps are greatly used in many applications these days. Axial-flow pumps are widely engaged in hydraulic engineering. So their performances should be important. This makes the industrial mans and researchers all over the world to think about the disorders that may interrupt these machineries. Parameters like turbulence and viscosity noticeably influence the flow in axial pumps. High pump revolution and complex geometry configuration along with blades tip clearance makes the flow non-uniform by producing vortexes. Today, having a probe into such hot topics is interesting using numerical and mathematical techniques. Paolo et. al. [1] reported an overview on previously offered pump models which took into account cavitation in different ways. Many researchers also worked on the evaluation of the flow inside the

*Corresponding author. E-mail: mfarhadi@nit.ac.ir

pump [2–5]. Zhang et al. [6] had a comparison between unsteady flow and experimental investigation in axial pump. They also confirmed that RNG k-ε turbulence model and SIMPLEC algorithm were effective in their work. Pressure fluctuation was the greatest at the inlet of the rotor in their study. Moreover, in recent years many researchers tried on simulation of flow field in axial pumps [7–10]. As fluid behavior is greatly affected by guide vanes installed after the pump impellers, the influence of adding guide vanes installed on the back of the axial flow pump needs to be further investigated [11–14]. Cavitation is a great disaster for turbo machines. This phenomenon which is an indication of pressure drop to under vaporization pressure puts negative and harmful effects on under water instruments like propellers and pumps. This phenomenon may greatly reduce the performance of a pump along with other undesirable events like noise, vibration and damages of components. Hence, many scientists are interested to research on cavitating flow characteristics. Numerical and analytical modeling are often used to predict the onset of the cavitation of a single bubble [15, 16], but rarely within a pump. There are some well-known models that can be used in describing the phenomena and behavior of the cavitation core [17 and 18]. To prevent erosion damages that possible cavitation occurrence can induce, the model should also be capable of accurately predicting cavitating flow phenomena [19]. A thorough review of cavitating flow simulation approaches is reported in [20]. Normally the simulations are based on two different concepts of modeling, the Euler–Euler approaches or the Euler–Lagrangian approaches. The basic flow of a liquid or liquid–gas mixture is computed in the Eulerian frame in both approaches using Finite-Volume methods for the Navier–Stokes or Euler equations of incompressible fluids [21]. Computational fluid dynamic uses these concepts widely and successfully in cavitation studies, and as a useful tool can give realistic results in cavitation simulations and predictions [22–27]. As discussed before, numerical methods and mathematical approach are widely used to capture the features of complex physical phenomenon. These tools help the researchers to overcome difficult problems. In this effort the 3D steady simulation of fully turbulent flow for axial cooling water pump of Mashhad power plant was handled using CFD commercial software FLUENT 6.3. Cavitation prediction was an issue to be discussed in this problem. The outcomes were depicted in pressure and velocity contour forms and also different streamlines for various situations were represented to observe the flow behavior. Also, the effect of flow rates on cavitation occurrence region was investigated.

2. GOVERNING EQUATIONS

For steady incompressible flows, the three-dimensional Reynolds-Averaged Navier-Stokes equations containing the mass and momentum conservation for this problem are defined through the following equations:

$$\frac{\partial}{\partial x_i}(\rho \bar{u}_i) = 0 \tag{1}$$

$$\frac{\partial}{\partial x_j}(\rho \bar{u}_i \bar{u}_j) = -\frac{\partial \bar{p}}{\partial x_i} + \frac{\partial}{\partial x_j}\left(\mu \frac{\partial \bar{u}_i}{\partial x_j} - \rho \bar{u}_i \bar{u}_j\right) \tag{2}$$

Where μ is the molecular viscosity, $-\rho \bar{u}_i \bar{u}_j$ is the Reynolds stress and $\bar{\rho}$ is the averaged pressure. The Reynolds stresses are modeled to clarify the context of eqn (2). So they are given by:

$$-\rho\overline{u}_i\overline{u}_j = \mu_t\left(\frac{\partial\overline{u}_i}{\partial x_j}+\frac{\partial\overline{u}_j}{\partial x_i}\right)-\frac{2}{3}\delta_{ij}\cdot\left(\rho k+\mu_t\frac{\partial\overline{u}_i}{\partial x_i}\right) \tag{3}$$

In which μ_t is the turbulent viscosity and k the turbulent kinetic energy. In turbulence models such as k-ε two additional transport equations should be solved to compute the turbulent viscosity. Turbulence kinetic energy, k, and turbulence dissipation rate, ε, must be evaluated in these equations.

2.1. RNG k-ε MODEL

A statistical technique named renormalization group theory was applied to support this turbulent problem. Since rotation and swirl in the mean flow put effect on turbulence, the RNG model which includes the effect of swirl on turbulence is applied and this enhanced the accuracy for swirling flow. Comprehensive details of RNG model characteristics and its applications in turbulence model can be found in Ref. [28]. The turbulence kinetic energy, k, and turbulence dissipation rate, ε, are given by following transport equations:

$$\frac{\partial(\rho k\overline{u}_i)}{\partial x_i} = \frac{\partial}{\partial x_j}\left(\alpha_k\mu_{eff}\frac{\partial k}{\partial x_j}\right)+G_k-\rho\varepsilon \tag{4}$$

$$\frac{\partial(\rho\varepsilon\overline{u}_i)}{\partial x_i} = \frac{\partial}{\partial x_j}\left(\alpha_\varepsilon\mu_{eff}\frac{\partial\varepsilon}{\partial x_j}\right)+\frac{C_{1\varepsilon}^*}{k}G_k-C_{2\varepsilon}\rho\frac{\varepsilon^2}{k} \tag{5}$$

Where and $\alpha_k = \alpha_\varepsilon = 1.393$ and $C_{2\varepsilon} = 1.68$. The production term in eqn (4) is given by:

$$G_k = \mu_t S^2 \tag{6}$$

In which S is the modulus of the mean rate of strain tensor:

$$S \equiv \sqrt{2S_{ij}S_{ij}},\ S_{ij} = \frac{1}{2}\left(\frac{\partial\overline{u}_i}{\partial x_j}+\frac{\partial\overline{u}_j}{\partial x_i}\right)$$

Additionally the effective viscosity is calculated by:

$$\mu_t = \rho C_\mu\frac{k^2}{\varepsilon},\ \mu_{eff} = \mu+\mu_t$$

With $C_\mu = 0.0845$ And:

$$C_{1\varepsilon}^* = C_{1\varepsilon}-\frac{\eta\left(1-\frac{\eta}{\eta_0}\right)}{1=\beta\eta^3},\eta = \left(2S_{ij}.S_{ij}\right)^{1/2}\frac{k}{\varepsilon} \tag{7}$$

$\eta_0 = 4.38$, $\beta = 0.012$, $C_{1\varepsilon} = 1.42$

3. BOUNDARY CONDITIONS

In this study the fluid is considered as incompressible and so no-slip condition was defined for all walls. The static vanes domain was solved in stationary reference frame while the impeller region which is implied as rotary part was solved in a moving reference of frame. The walls separating the stationary and the rotary parts are prescribed as interior faces. For the inlet and outlet of the solution domain constant velocity inlet normal to boundary and pressure outlet were chosen, respectively.

3.1. MOVING REFERENCE FRAME (MRF) TECHNIQUE AND NUMERICAL METHOD

Moving reference frame (MRF) is employed to solve the pump impeller region which is attached to a rotating frame work. The rotational domain includes the impellers and the volume around them in a circular manner. This domain was treated first. Getting some results from this domain, the interface between this domain and the stationary domain would be a boundary condition to transfer these results to solve the stationary domains. In this paper commercial CFD software FLUENT 6.3 was utilized for all simulations. A pressure based finite volume method was used in this effort. Three-dimensional steady-state incompressible fluid equations were solved. RNG k-ε model was utilized for modeling turbulence. Also, SIMPLEC algorithm was used for the pressure velocity coupling. For the equations of momentum, turbulence kinetic energy and turbulence dissipation rates, the second order upwind difference scheme was used. Monitoring the rate of change for each dependent variable the convergence of the solution was checked. When the rates decreased to fewer than three orders of magnitude, the solution was considered to be converged.

4. GEOMETRY AND GRID GENERATING

In order to have sufficient control on physical events, the whole hydraulic passage of the axial pump should have been modeled and the model is shown in fig. 1. Initially for modeling such complex geometry, CFTurbo software which was based on the techniques and information about pump characteristics was utilized. This software designed the profiles of the blades according to the existing data from Mashhad power plant which is the reference of this study. The next step for simulation needed mesh generating for the geometry. For this purpose the model was exported to Gambit software and the model was fulfilled there. After essential considerations on modeling and mesh generating, the model was finally simulated by FLUENT software. The two definite zones were perfectly simulated. The first zone

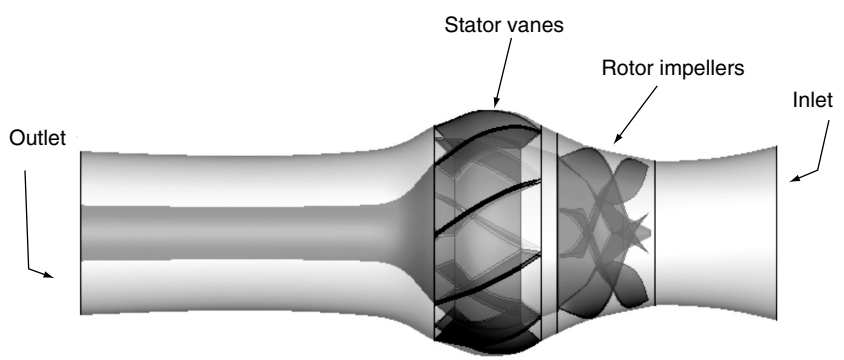

Figure 1 Pump impellers and stator vanes.

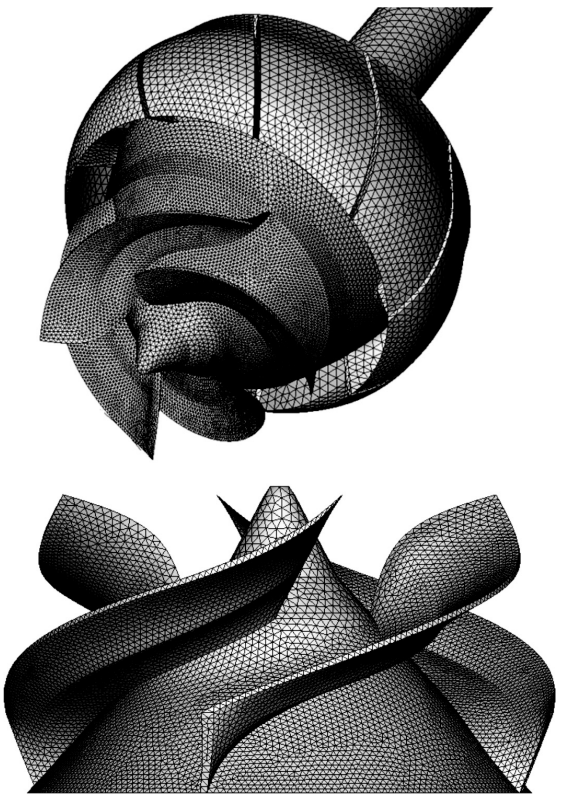

Figure 2 Mesh of the geometry.

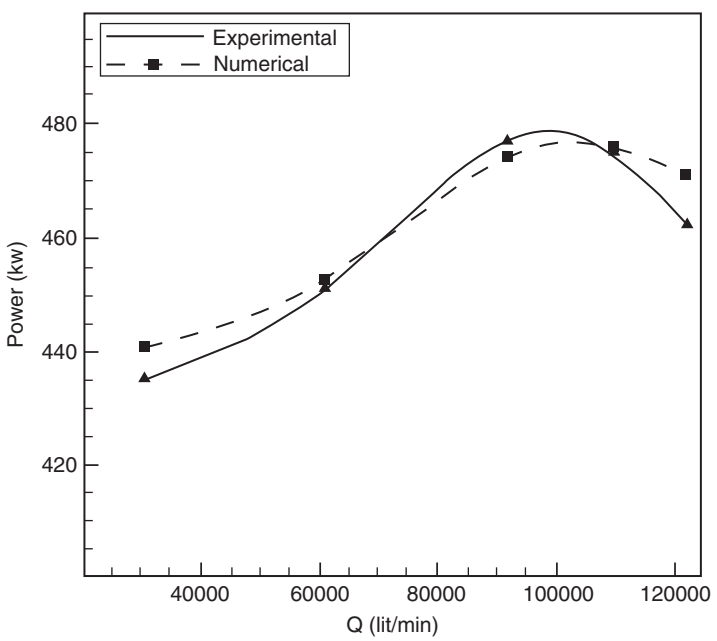

Figure 2 Comparison of the reference and simulated pump performance curve.

contained the impellers and the rotary parts which were solved in a moving framework. The second one included the guide vanes and the stationary parts like inlet and outlet regions which were treated in a stationary framework. 4 axial flow blades mounted on a conical hub provided the rotary zone there were 9 stator vanes afterward. The hub diameter and the impeller diameter were 167 and 766 mm, respectively.

Difficulties of the geometry of the problem imposed using hybrid meshing scheme through tetrahedral cells in the solution domain. Logically, for better capturing the events in critical regions, finer meshes were used in areas near the moving impellers and the rotary zone. The way the geometry is meshed can be important for a precise solution. So mesh independency of the results was verified through analyzing the effect of mesh number on parameters like power and static pressure rise.

5. RESULTS

Defining a proper solution grid and sufficient boundary condition which best suites the problem and its equations, in this step the simulation results are represented. Fig 3 is a comparison of the simulated pump performance curve and the experimental case. As it is obvious delightful agreement exists in this feature. This means that the way the problem is dealt with was correct and the numerical method which handled this problem was sufficiently selected. Numerical procedures contain some assumptions which yield to a little difference between numerical solution and the experimental cases.

Fig 4 & 5 show the pressure contour and velocity contour, respectively. From these contours two main parameters can be noticed. First, as the impellers transfer energy to the passing fluid, the fluid in this region has the most amount of velocity and according to Bernoulli's equation this is a sign of pressure drop for this criterion. This pressure drop can cause problem which is discussed in following parts. Second, this turbulent flow which passes the impellers has strong swirling behavior and this means having high kinetic energy and subsequently high amount of hydraulic loss. Normally guide vanes are

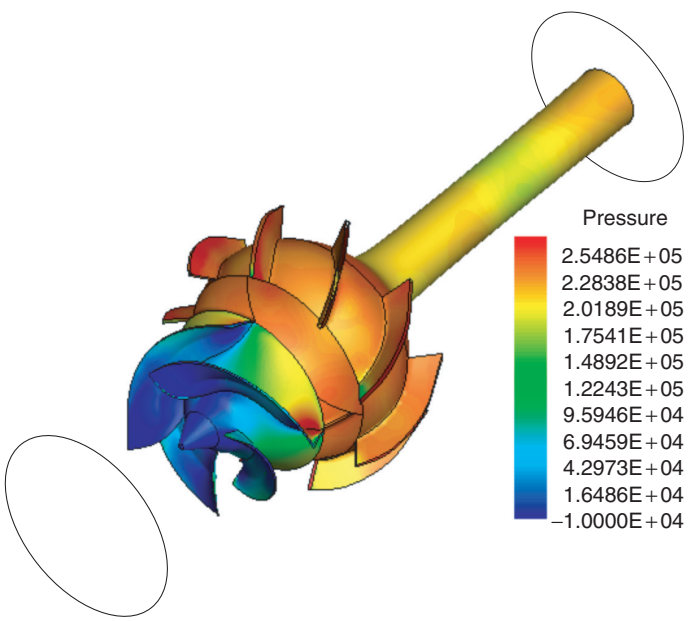

Figure 3 Pressure contour of the pump.

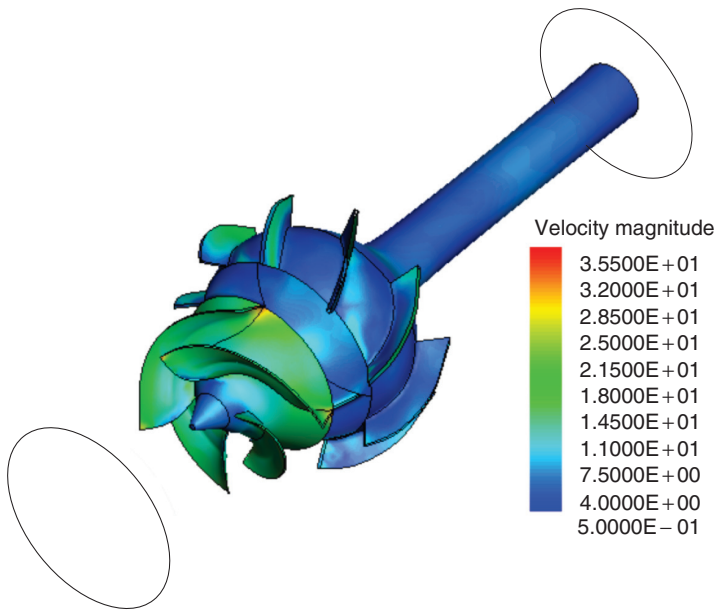

Figure 4 Velocity contour of the pump.

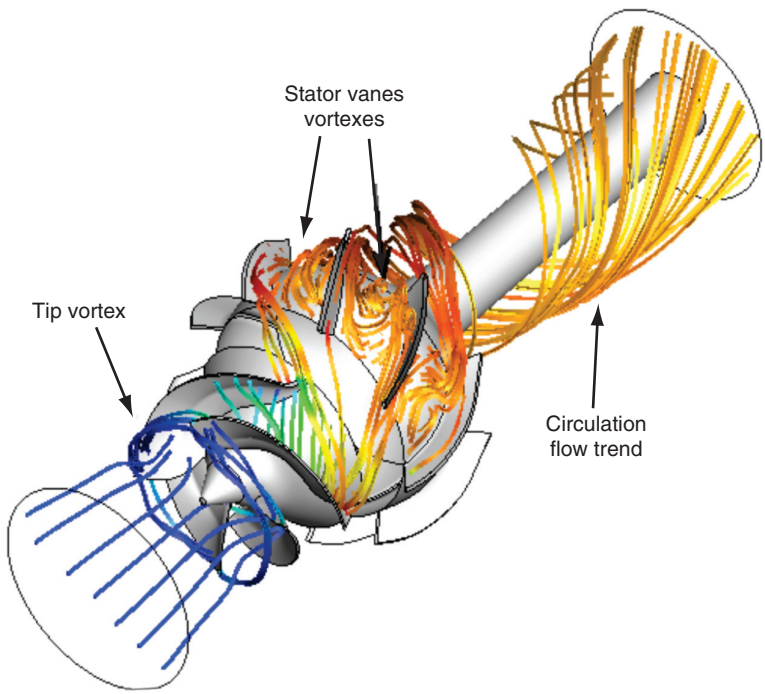

Figure 5 Streamlines of the whole solution domain.

designed to convert kinetic energy to pressure energy by guiding the flow. This reduces the hydraulic loss and as a result makes the stator vane region as a high pressure region in the whole domain. This high pressure region is clearly seen in the pressure contour. Passing

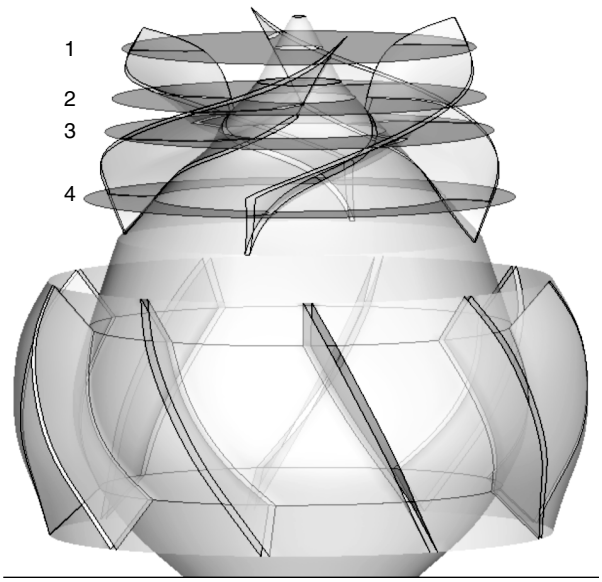

Figure 6 The planes which cut the impellers.

through the guide vanes the fluid reaches the outlet with a slight decrease in the pressure which is lost in the duct.

Fig 6 is a demonstration of flow behavior through its streamlines. Fully swirling flow can be easily seen in this figure. As the fluid gets swirling velocity from the impellers, it follows the trend to the end of the domain despite the existing guide vanes. Two types of vortexes can be noticed. Tip vortexes are made due to the small clearance of blades tip and the shell covering them and the velocity of the fluid. In the next part because of energy transformation in stator domain, high pressure regions are formed adjacent to low pressure regions existing near the root of static blades and this results to having back flow and finally some vortexes in that region.

In order to have better viewpoint to the flow behavior and the way different parameters put effect on it, the impellers domain was cut through four planes and the flow behavior in these planes was analyzed by applying streamlines. The planes are placed in 4 different sections of the blades for better investigation of flow pattern over the blades as it can be seen in figure 7. The case was treated for different flow rates and different pump speeds.

Different flow rates were defined by different pump inlet velocity of the fluid and so they are named in this way. Figure 8 shows streamlines in these four sections for inlet velocities of 1, 2, 3, 3.58 and 4 m/s. The pump speed was assumed to be constant for this part (743 rpm). Figures confirm that for the lowest flow rate (inlet velocity of 1 m/s) because of lack of the fluid amount in comparison with the needed amount for that special speed, strong swirling flow immerges in the first section, since it was near the leading edge of the blade and great suction governed that region. In other sections the flow behaved normally and no sensible chaos was observed. For the inlet velocity of 2 m/s it is seen that enhancing the inlet velocity emitted the circulating behavior and the flow got normal behavior in all sections. Following the streamlines for inlet velocity of 3 m/s, it can be said that the flow tended to make some vortexes near the leading edge of the blades. Increasing the inlet velocity approaches more to the turbulent flow and as a result

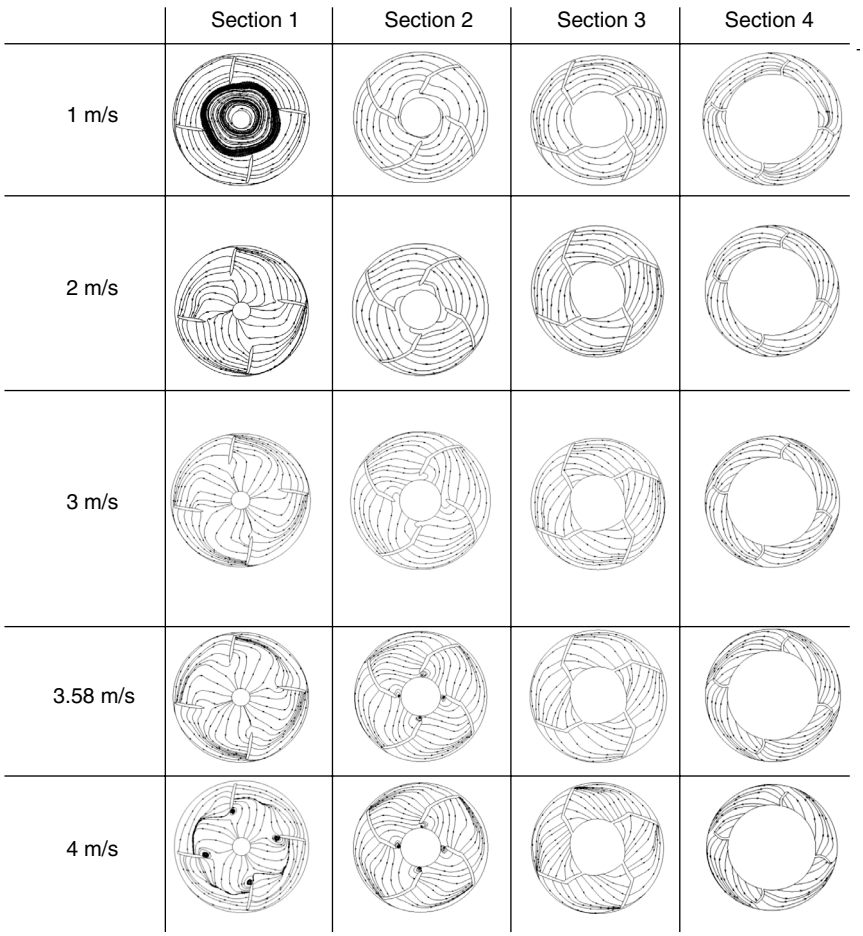

Figure 7 4 sections streamlines for different inlet velocities.

vortex appearance is expected. For velocity of 3.58 m/s it is seen that small vortexes appeared in section 2 and for velocity of 4 m/s which was more than optimum velocity of that ump speed turbulent vortexes became more in section 1 and 2. It is noteworthy to say that in all cases the flow near the trailing edge of the blades i.e. sections 3 and 4 behaved smoothly with no vortex.

Figure 9 represents streamlines for the four sections discussed former for pump speed of 500, 600, 743, 800, 900 and 1000 rpm. In this part the flow rate which was defined by the inlet velocity was constant with velocity of 3.58 m/s (optimum velocity). The streamlines for speed of 500 rpm showed that when pump speed was not as high as the sufficient amount for that flow rate, the flow experienced some vortexes in the first and second sections of the blades. The reason is that the pump couldn't afford that amount of fluid with that speed. When sufficient energy was not transferred to the fluid, low pressure regions appear in suction sides of the blades near the leading edge and as a result vortexes take form. By increasing the pump speed it is seen that vortexes became weaker and by reaching the nominal speed of 743 rpm the vortexes of first section disappeared, but still some vortexes existed at the second section. Enhancing the speed more and more, vortexes vanished slightly and in speed of 900 rpm it is seen that no vortex exist anymore. Again for speed of 1000 rpm

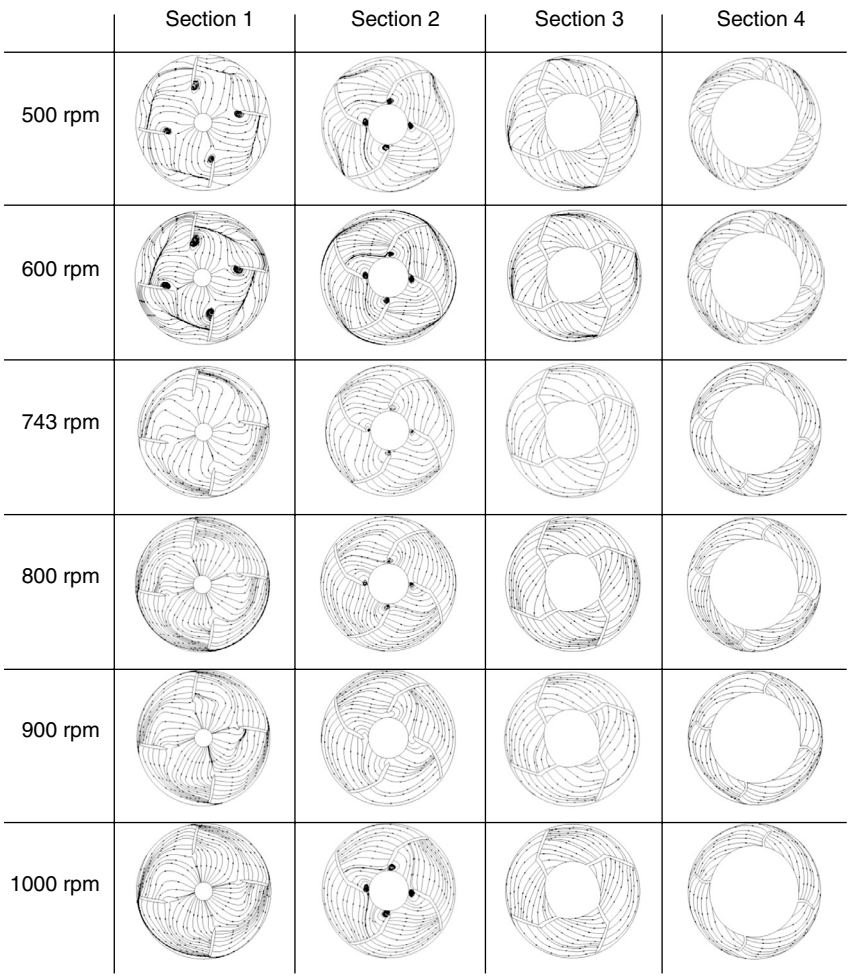

Figure 8 4 sections streamlines for different pump speeds.

it is seen that some vortexes appeared because of high angular velocity transformed to the fluid in that high speed. It is remarkable that the second half of the blades experienced no vortexes in any cases.

Iso-surface contours were applied to have a clear probe into cavitation phenomenon. Figure 10 demonstrates the effect of the flow rate passing the pump system on cavitaion occurrence. Repeatedly in this section the flow rate is introduced using the inlet velocity. For this case the velocity of 1, 2, 3, 3.58 and 4 m/s are agent for the flow rate of 30600, 61200, 91800, 109800 and 122000 lit/min, respectively. Contemplating the results, it is concluded that for the lowest flow rate the cavitation region appear at the top of the conic part. That region is the start point for this phenomenon. Enhancing the flow rates conducted the saturation region toward the lower parts of the leading edge of the blades and it is confirmed by pressure contours when they introduce the regions which experience pressure drops. Gradually cavitation region moved toward blades surface and placed on the suction side of the blades. It is seen that for the optimum inlet velocity which best suits the pump speed cavitation region is smaller than other situations. Enhancing the inlet velocity more, helped

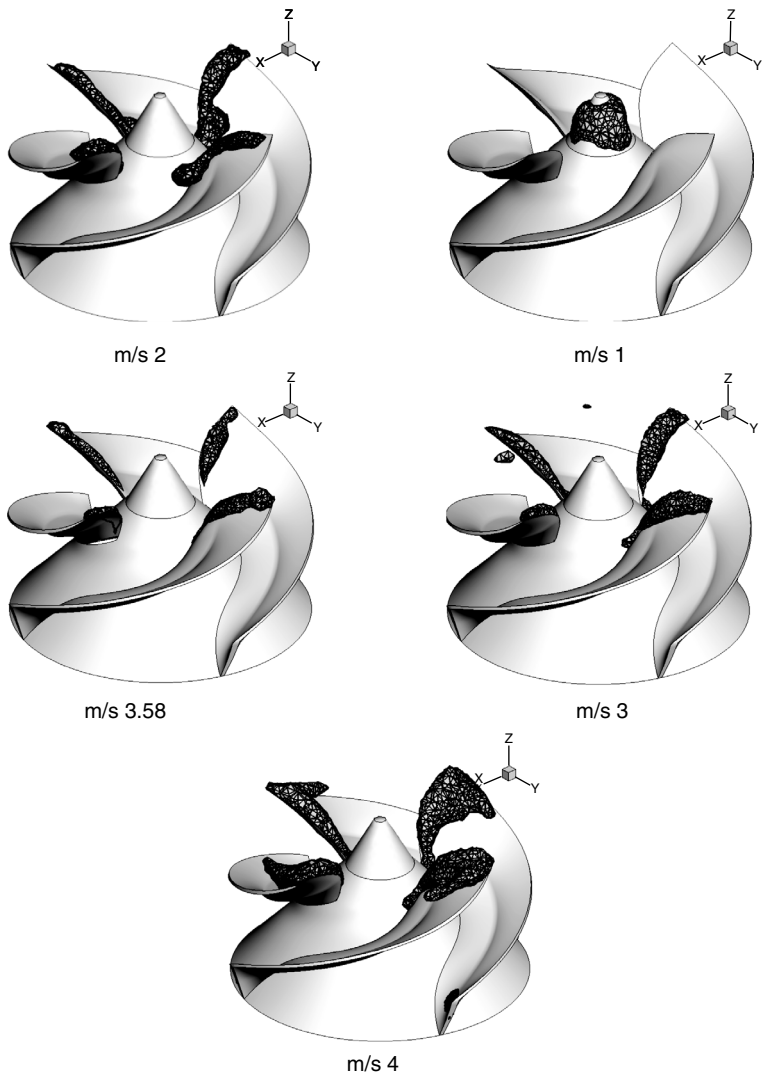

Figure 9 Iso-surface contour of cavitation occurrence.

to the appearance of vortexes which was discussed former, and consequently low pressure regions took form in suction side of the blades and finally the cavitation region grew more. It should be noticed that for the flow rate of more than the optimum amount (109800 lit/min) cavitation region appeared on the trailing edge of the blades and this means that the pump exposes more damages in such situations. Also it should be noted that when it is talked about cavitation phenomenon all 3D space of the domain should be considered, not just the surfaces. As it is observed in the 3D contours that cavitation region engages volumes of fluid.

6. CONCLUSION

In regard to the results of this study it can be said that the numerical technique and mathematical algorithm utilized to deal with this problem worked delightfully. RNG k-ε model handled the turbulence behavior and swirl pattern of the flow in a good way. Also

MRF technique treated well with the stator and rotor interaction and as a result good agreement was observed in the performance curve between the simulated pump and the experimental case of the power plant. Due to maximum rotational speed plus small tip clearances of the blades, tip vortexes formed at the tip of the blades. Energy transform from kinetic to pressure energy in stator vanes yielded to the formation of backflow region and consequently vortexes appeared in that area. The streamlines for different sections of the blades show that for situations far from the optimum operation condition, vortexes may appear and the fluid would behave in an unwanted manner. The leading edge of the blades on the suction side exposes more vortexes and low pressure regions and the risk of cavitation formation is more in this region. The flow rate had remarkable effect on cavitation occurrence. Using CFD approach, regions which experience cavitation can be predicted in different situations and in this way the designers would know the places where need more resistant material for cavitation erosion prevention.

REFERENCES

[1] Paolo C. Andrea V. Germano F. Gian L. B, Modeling of fluid properties in hydraulic positive displacement machines, *Simulation Modeling Practice and Theory*, 2006, 14, 1059–1072.

[2] Harrison, A.M. Edge, K.A. Reduction of axial piston pump pressure ripple, *Proceedings of the Institution of Mechanical Engineers, Part I: Journal of Systems and Control Engineering*, 2000. 214 (1), 53–63.

[3] Johansson, A. Andersson, J. Palmberg, J.O. Optimal design of the cross-angle for pulsation reduction in variable displacement pumps, *Proceeding of Bath Workshop on Power Transmission and Motion Control*, University of Bath, UK, 2002.

[4] Gian, L. B. Paolo, C. Andrea, V. Guidetti, M. Simulation model of axial piston pumps inclusive of cavitation, *ASME International Mechanical Engineering Congress and Exposition*, New Orleans, Lousiana, USA, November, 2002. 29–37.

[5] Paolo, C. Abdrea, V. Modeling of an axial piston pump for pressure ripple analysis. *In: Proc. of The 8th Scandinavian Int. Conference on Fluid Power*, Tampere Finland, May 7–9, 2003.

[6] ZHANG, D. Sh. SHI, W. D. CHEN, B. GUAN, X. UNSTEADY FLOW ANALYSIS AND EXPERIMENTAL INVESTIGATION OF AXIAL-FLOW PUMP, *Journal of Hydrodynamics*, 2010, 22(1):35–43.

[7] SHIGMITSU, T. FURUKAWA, A. and WATANABE S. et al. Internal flow measurement with LDV at design point of contra-rotating axial flow pump Nihon Kikai Gakkai Ronbunshu. *Transactions of the Japan Society of Mechanical Engineers, Part B*, 2008, 74(5): 1091–1097 (in Japanese).

[8] GAO, H. LIN, W. L. and DU Z. H. An investigation of the flow and overall performance in a water-jet axial flow pump based on computational fluid dynamics and inverse design method. *Proceedings of the Institution of Mechanical Engineers, Part A: Journal of Power and Energy*, 2008, 222(5): 517–527.

[9] FAN, H. HONG, F. and ZHOU, L. D. et al. Design of implantable axial-flow blood pump and numerical studies on its performace. *Journal of Hydrodynamics,* 2009, 21(4): 445–452.

[10] HUANG, H. M. GAO, H. and DU, Z. H. Numerical simulation and experimental study on flow field in an axial flow pump. *Journal of Shanghai Jiaotong University*, 2009, 43(1): 124–128 (in Chinese).

[11] Naqvi, R. Wolf, J. Bolland, O. Part-load analysis of a chemical looping combustion (CLC) combined cycle with CO2 capture. *Energy*, 2007, 32, 360–370.

[12] Kim, K.T., Suh, J.M. Development of an advanced PWR fuel for OPR1000s in Korea. *Nuclear Engineering and Design*, 2008, 238 (10), 2606–2613.

[13] Kim, K.T., Jang, Y.K., Kim, J.I., 2009. The study on the impact of fsi on the fuel assembly design optimization. *ASME Pressure Vessels and Piping Conference*, Chicago, Illinois, USA, 2008, 4, 15–19.

[14] Chi, J.L., Wang, B., Zhang, S.L., Xiao, Y.H. Off-design performance of a chemical looping combustion (CLC) combined cycle: effects of ambient temperature. *Journal of Thermal Science*, 2010. 19 (1), 87–96.

[15] Li SC. *Cavitation of hydraulic machinery*. London: Imperial College Press; 2000.

[16] Edward, G. *Cavitation and the centrifugal pump: a guide for pump users*. Philadelphia (PA): Taylor & Francis; 1999.

[17] Uchiyama T. Numerical simulation of cavitating flow using the upstream finite element method. *Applied Mathematical Modelling*, 1998, 22; 235–50.

[18] Michelle, F. Some present trends in hydraulic machinery research. *Hydraulic machinery and cavitation*. London: Kluwer Academic Publishers; 1996.

[19] Catania, A.E. Ferrari, A. Spessa, E. Temperature variations in the simulation of high-pressure injection-system transient flows under cavitation, *International Journal of Heat and Mass Transfer*, 2008, 51, 2090–2107.

[20] Catania, A.E. Ferrari, A. Manno, M. Spessa, E. A comprehensive thermodynamic approach to acoustic cavitation simulation in highpressure injection systems by a conservative homogeneous two-phase barotropic flow model, *ASME Journal of engineering for gas turbines and power*. 2006, 128 (1-2), 434–445.

[21] Abdel-Maksoud, M. Hänel, D. Lantermann, U. Modeling and computation of cavitation in vortical flow, *International Journal of Heat and Fluid Flow*, 2010, 31, 1065–1074.

[22] LIU, D. M. LIU, S. H. and WU, Y. L. et al. LES numerical simulation of cavitation Bubble shedding on ALE 25 and ALE 15 hydrofoils. *Journal of Hydrodynamics*, 2009, 21(6): 807–813.

[23] WANG, G. OSTOJA, S. M. Large eddy simulation of a sheet/cloud cavitation on a NACA0015 hydrofoil. *Applied Mathematical Modelling*, 2007, 31(3): 417–447.

[24] POUFFARY, B. PATELLA, R. F. and REBOUD J. L. et al. Numerical simulation of 3D cavitating flows: Analysis of cavitation head drop in turbomachinery. *Journal of Fluids Engineering*, 2008, 130: 061301.

[25] PARK, K. SEOL, H. and CHOI W. et al. Numerical prediction of tip vortex cavitation behavior and noise considering nuclei size and distribution. *Applied Acoustics*, 2009, 70(5): 674–680.

[26] HATTORI, S. KISHIMOTO, M. Prediction of cavitation erosion on stainless steel components in centrifugal pumps. *Wear*, 2008, 265(11–12): 1870–1874.

[27] YE, J.M. XIONG, Y. Prediction of podded propeller cavitation using an unsteady surface panel method. *Journal of Hydrodynamics*, 2008, 20(6): 790–796.

[28] WANG, F. J. *Computational fluid dynamic analysis- CFD principle and application*. Beijing: Tsinghua University Press, 2004, 114–116 (in Chinese).